Magnetic-Field-Induced Rotation of Polarized Light Emission from Monolayer WS_2

Robert Schmidt,[1] Ashish Arora,[1] Gerd Plechinger,[2] Philipp Nagler,[2] Andrés Granados del Águila,[3,†] Mariana V. Ballottin,[3] Peter C. M. Christianen,[3] Steffen Michaelis de Vasconcellos,[1] Christian Schüller,[2] Tobias Korn,[2] and Rudolf Bratschitsch[1,*]

[1]*Institute of Physics and Center for Nanotechnology, University of Münster, 48149 Münster, Germany*

[2]*Department of Physics, University of Regensburg, 93040 Regensburg, Germany*

[3]*High Field Magnet Laboratory (HFML—EMFL), Radboud University, 6525 ED Nijmegen, The Netherlands*

(Received 29 April 2016; published 12 August 2016)

We control the linear polarization of emission from the coherently emitting K^+ and K^- valleys (valley coherence) in monolayer WS_2 with an out-of-plane magnetic field of up to 25 T. The magnetic-field-induced valley Zeeman splitting causes a rotation of the emission polarization with respect to the excitation by up to 35° and reduces the polarization degree by up to 16%. We explain both of these phenomena with a model based on two noninteracting coherent two-level systems. We deduce that the coherent light emission from the valleys decays with a time constant of $\tau_c = 260$ fs.

DOI: 10.1103/PhysRevLett.117.077402

Atomically thin transition metal dichalcogenides (TMDCs), such as MoS_2, represent a new class of semiconductors [1–3]. Their band structure exhibits an indirect to direct band gap transition, when the thickness is reduced to a monolayer (ML) [4–10]. The associated optical transitions are located at the K^+ and K^- points of the Brillouin zone [11–15]. The strong spin-orbit interaction combined with the broken inversion symmetry in a ML leads to distinct optical selection rules for the K^+ and K^- valleys. Excitation with left (right) circularly polarized light predominantly results in the photoluminescence emission of left (right) circularly polarized light ("valley polarization") [11–15]. For excitation with linearly polarized light, the radiation emitted from a ML under near-resonant excitation also has linear polarization oriented in the same direction as the polarization of the laser but only to a degree of ≈30%. This effect has been attributed to a superposition of coherently emitted σ^+ and σ^- polarized light from the K^+ and K^- valleys and has been termed "valley coherence" [16–18]. These properties render TMDCs promising candidates for optoelectronic applications such as LEDs [19–21], single-photon emitters [22–26], or conceptually new valleytronic devices [27].

Since it is extremely difficult to control light with a magnetic field in vacuum [28], magnetic [29–31] or conventional semiconducting [32] solid-state materials are widely used to mediate the interaction. In atomically thin semiconductors, an external magnetic field lifts the energy degeneracy of the K^+ and K^- valleys [Fig. 1(a)] by the so-called "valley Zeeman effect" [23,33–39]. It results in a redistribution of carriers in the two valleys due to intervalley scattering causing a magnetic-field-induced valley polarization [34–36,38]. Also, it reduces the degree of linear polarization of emitted light in ML WSe_2 under linearly polarized excitation [34,37]. Here, we measure the photoluminescence of ML WS_2 at cryogenic temperatures ($T = 4.2$ K) using linearly polarized light for excitation, in magnetic fields up to 30 T applied in Faraday geometry. Interestingly, we find that the relative angle between the polarization of the laser used for excitation and the photoluminescence emission of the A exciton drastically changes with an increasing magnetic field, accompanied with a decreasing polarization degree of emission. This behavior is explained with a model based on the coherent emission of σ^+ and σ^- polarized radiation from the Zeeman-split K^+ and K^- valleys. From our analysis, we deduce that the coherent emission from the valleys decays with a time constant of $\tau_c = 260$ fs.

WS_2 MLs are obtained by the mechanical exfoliation of single crystals onto a $SiO_2(285\ \mathrm{nm})/\mathrm{Si}$ substrate. They are identified using optical microscopy and microphotoluminescence (μPL) spectroscopy [40]. Figure 1(b) depicts the helicity-resolved μPL of the neutral A exciton at a temperature of 4.2 K and magnetic fields up to $B = 30$ T in Faraday geometry [wave vector $\vec{k}$ parallel to $\vec{B}$; see the inset in Fig. 1(d)] under linearly polarized excitation (2.21 eV). The σ^+ and σ^- components of the μPL are resolved using a combination of a quarter wave plate and a linear polarizer. The exciton transition energies $E_{K^\pm}$ are obtained by fitting the μPL spectra with Lorentzians. The valley Zeeman splitting for excitons ΔE is $E_{K^+} - E_{K^-} = g_X \mu_B B$, with the effective A exciton g factor g_X and Bohr magneton μ_B. We observe an increasing splitting with rising B [Figs. 1(c) and 1(d)]. A linear fit to the data in Fig. 1(d) provides an exciton g factor of $g_X = -4.3$, which is in good agreement with a recently reported value for CVD-grown WS_2 [39].

To analyze the effect of the magnetic field on the valley coherence, the polarization state of the emitted light at the A exciton resonance is measured for a fixed linearly polarized excitation. The emission is analyzed for linear polarization, while the μPL spectra are measured in steps of 10°, covering the full 360° of the analyzer angle. The Faraday rotation of the linear polarization caused by optical elements is compensated by appropriately rotating the excitation polarizer

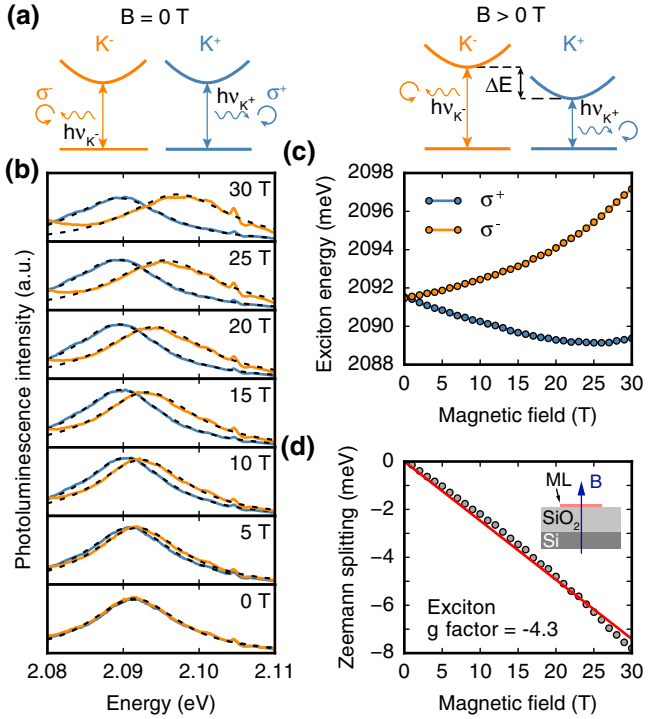

FIG. 1. (a) Illustration of the circularly polarized PL emission from the two valleys, without and with an applied magnetic field. (b) Right (σ^+, blue lines) and left (σ^-, orange lines) circularly polarized photoluminescence components from the A exciton of monolayer WS_2 at a temperature of 4.2 K for different magnetic fields under linearly polarized excitation. The dashed curves indicate line shape fits to the data. The feature at 2.105 eV is an artifact originating from the spectrometer and CCD. (c) σ^+ and σ^- polarization-resolved exciton transition energies and (d) Zeeman splitting of the A excitons (circles) as a function of the magnetic field, with a linear fit (red line). The inset shows the sample geometry.

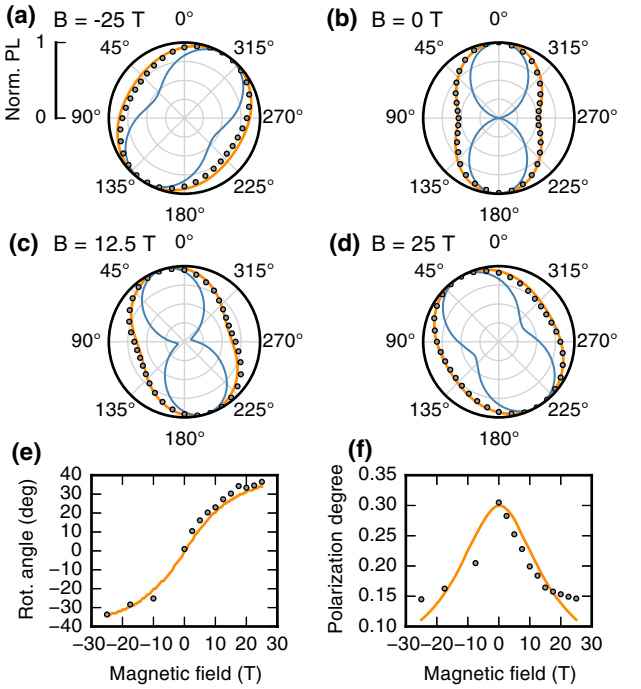

FIG. 2. (a)–(d) Measured normalized photoluminescence intensity (solid circles) for monolayer WS_2 as a function of the analyzer angle, under linearly polarized excitation for different magnetic fields. The blue lines indicate the polarization patterns obtained from our model of the coherent component of the emission, excluding the incoherently emitted background. (e) Relative rotation angle between the excitation and emission polarization for different magnetic fields. (f) Linear polarization degree of the emission as a function of the magnetic field. The orange lines in (a)–(f) show the global fit to the data for all measured magnetic fields, using the model described in the text.

(see Supplemental Material [41]). Figures 2(a)–2(d) depict the integrated PL intensities of the A exciton as a function of the analyzer angle for different magnetic fields up to 25 T [see Supplemental Material (Fig. S1) for all measured fields [41]]. An angle of zero degrees denotes no rotation and is identical to the polarization direction of the pump laser. From Figs. 2(a)–2(d), two effects are evident. Most notably, the relative angle between the excitation and emission polarization drastically changes with the magnetic field [Fig. 2(e)]. For $B = 0$ T, the emission polarization has the same direction as the excitation (valley coherence effect) [16]. However, for $B \neq 0$ T, the emission polarization direction rotates with respect to that of the excitation. In addition to the rotation, the linear polarization degree decreases with an increasing magnetic field [Fig. 2(f)]. The polarization degree is defined as $(I_{\max} - I_{\min})/(I_{\max} + I_{\min})$, where $I_{\max}$ and $I_{\min}$ are the maximum and minimum intensities, respectively.

To understand these two striking effects, we analyze the exciton dynamics in the K^+ and K^- valleys, assuming that at time $t = t_0$ a linearly polarized excitation (polarization axis y) creates an equal population of excitons in both valleys. We find in the experiment that the emitted radiation is only partially polarized (30% for $B = 0$ T), which is in agreement with previous measurements [16,17]. Therefore, we assume that the measured photoluminescence is a superposition of coherently emitted radiation with intensity I_c and an incoherently emitted background with intensity I_b, with the fraction of incoherent emission given by $b = I_b/(I_c + I_b)$. While the coherently emitted radiation gives rise to the observed linear polarization, we expect the incoherent part to be unpolarized. To analyze the polarization behavior with an applied magnetic field, we describe the electric field associated with the circularly polarized, coherent part of the emission from the two valleys by damped harmonic oscillators, written in the Jones' vector form:

$$\vec{\mathcal{E}}_{K^\pm}(t) = \mathcal{E}_0 e^{-(t/2\tau_c)} \begin{pmatrix} \mp \cos\left(\frac{E_{K^\pm}}{\hbar} t\right) \\ \sin\left(\frac{E_{K^\pm}}{\hbar} t\right) \end{pmatrix}, \quad (1)$$

where $\mathcal{E}_0$ denotes the amplitude of the emitted electric field at $t = t_0$. The electric field is assumed to decay monoexponentially with a characteristic damping time τ_c. The resulting electric field of the emitted light from the ML

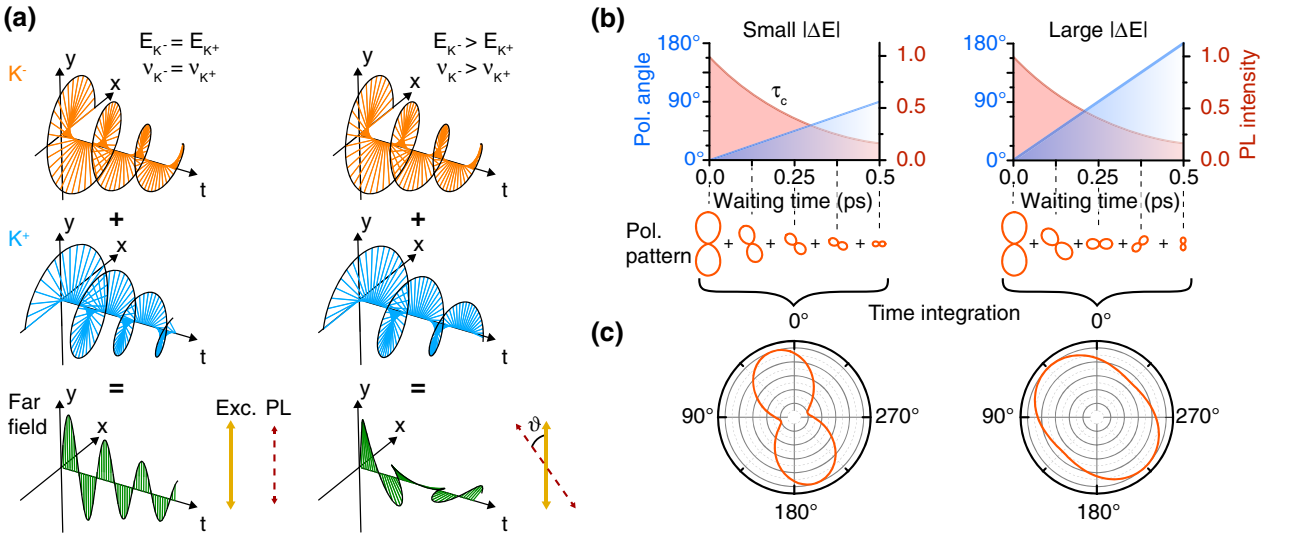

FIG. 3. (a) Illustration of the decaying E fields of the circularly polarized emission from the K^+ and K^- valleys. For $B = 0$ T, the far-field superposition from both valleys results in a linearly polarized wave. For $B \neq 0$ T, the different frequencies emitted from the valleys cause a slowly rotating linear polarization during the photoluminescence decay. Solid and dashed arrows (bottom) depict the polarization directions of excitation and time-integrated emission. (b) and (c) represent two cases for a small and a large Zeeman splitting $|\Delta E|$. The decay dynamics are assumed to be equal in the two cases depicted in (b), while the rate of rotation of the linear polarization scales with $|\Delta E|$. A larger $|\Delta E|$ leads to a large rotation of the linear polarization of the time-integrated emission, accompanied by a strong decrease in the degree of polarization as illustrated in (c).

measured at the detector will be the far-field superposition of the σ^+ and σ^- emission components from the K^+ and K^- valleys, respectively. It is calculated by the vector addition of Eq. (1) for the two valleys:

$$\vec{\mathcal{E}}(t) = 2\mathcal{E}_0 e^{-(t/2\tau_c)} \sin\left(\frac{E_{K^+} + E_{K^-}}{2\hbar} t\right) \begin{pmatrix} \sin\left(\frac{\Delta E}{2\hbar} t\right) \\ \cos\left(\frac{\Delta E}{2\hbar} t\right) \end{pmatrix}. \quad (2)$$

Therefore, the electric field in the far-field superposition contains two frequencies with a fast component $(E_{K^+} + E_{K^-})/(2\hbar)$, which depends weakly on the magnetic field, and a strongly magnetic-field-dependent slow component $\Delta E/(2\hbar) = (E_{K^+} - E_{K^-})/(2\hbar)$, where ΔE is the excitonic Zeeman splitting. In the absence of a magnetic field, both valleys are degenerate ($\Delta E = 0$) [Figs. 1(a) and 3(a), left]. In this case, the emitted electric field is linearly polarized along the y direction, which is also the polarization direction of the excitation laser [bottom of Fig. 3(a) and Fig. 2(b) in our experiment]. In the presence of a magnetic field, the valley degeneracy is lifted ($\Delta E \neq 0$) [Figs. 1(a) and 3(a), right]. The factor involving ΔE in Eq. (2) causes a slow rotation (when compared to the frequency of the emitted light) of the linear polarization over the course of the decay with a frequency of $\Delta E/(2\hbar)$ [Fig. 3(a), right]. In a quantum mechanical picture, this slow rotation represents the phase difference between the excitons in the K^+ and K^- valleys. The polarization pattern of the time-integrated emission is given by the sum of all polarization patterns at various times during the decay, taking their corresponding intensities into account. In effect, the slow temporal rotation of linear polarization in the presence of a magnetic field causes a rotation of the time-integrated polarization state with respect to the zero field case, accompanied with a loss of polarization degree. In Figs. 3(b) and 3(c), we present two cases with a small and a large $|\Delta E|$. In the former case, the polarization vector rotates slower than the latter, as shown by the patterns at different times over the course of decay in Fig. 3(b). Since the decay time is equal for both cases, a larger $|\Delta E|$ causes more rotation and a greater loss of polarization degree [Fig. 3(c)]. In previous experiments, this decrease of linear polarization with the magnetic field was interpreted in context of a Hanle experiment and attributed to dephasing processes [34]. In our case, the reason for the decrease of polarization degree with an increasing magnetic field is the rotating polarization in the far-field superposition of the emission instead of fast exciton dephasing.

For a quantitative simulation of the analyzer-angle-resolved light intensity for a given magnetic field B, the rotating electric field $\mathcal{E}(t)$ is projected on the transmission axis of the analyzer at an angle ϑ, which yields the angle-dependent electric field $\mathcal{E}_\vartheta(t)$. $[\mathcal{E}_\vartheta(t)]^* \mathcal{E}_\vartheta(t)$ is integrated over time to obtain $I_{c,\vartheta}$, which is proportional to the coherently emitted photoluminescence intensity as a function of analyzer angle ϑ. The measured intensity is given by the sum of $I_{c,\vartheta}$ and $I_b/2$:

$$I(\vartheta) = I_{c,\vartheta}(\vartheta) + \frac{I_b}{2} = \int_0^\infty [\vec{\mathcal{E}}_\vartheta(t)]^* \vec{\mathcal{E}}_\vartheta(t) dt + \frac{I_b}{2}, \quad (3)$$

where the factor $\frac{1}{2}$ in $(I_b/2)$ accounts for the fraction of unpolarized background transmitted through the analyzer. The orange lines in Fig. 2 represent a global fit of our model to the measured data with τ_c and b as the free parameters, while E_{K^+} and E_{K^-} are obtained from Fig. 1. The blue lines show the polarization patterns without an included incoherent background I_b. A deviation from the ideal dipole pattern (i.e., for $B = 0$ T) shows the effect of magnetic-field-induced depolarization for $B \neq 0$ T. Our model is in excellent agreement with the experimental data. The values obtained from the global fit are $\tau_c = (260 \pm 5)$ fs and $b = (70 \pm 0.3)\%$. The decay time τ_c describes the damping of the coherently emitted radiation, which may originate from the decay of the exciton population as well as dephasing of the excitons in the single valleys. Hence, $(1/\tau_c)$ can be expressed as the sum of the inverse of the population decay time $(1/2\tau_{\mathrm{pop}})$ and the inverse of the pure exciton dephasing time $(1/\tau_{\mathrm{dphs}})$ [42]. τ_c is comparable to the T_2 time of 250 fs, measured in photon echo experiments of a WSe_2 monolayer [42]. In addition, it has been shown that excitons in the light cone undergo ultrafast radiative recombination with a lifetime of about 150 fs in a WSe_2 monolayer using time-resolved terahertz spectroscopy [43]. In another study, a valley coherence decay time of 100 fs was measured in a WSe_2 monolayer using 2D coherent spectroscopy [44]. These values obtained for WSe_2 are of the same order of magnitude as our derived value in a WS_2 monolayer and recent theoretical predictions [45]. A significant fraction of the light emission arises from excitons scattered out of and back into the light cone due to intravalley scattering, causing much longer decay times (2–3 orders of magnitude) [43]. We believe that these excitons lose their phase information, whereas excitons directly recombining within the light cone emit coherently. Together with additional intervalley scattering, these processes contribute to the incoherently emitted background. This scenario is consistent with the obtained value for the incoherent background of 70%; i.e., only 30% of the excitons participating in the radiative recombination processes emit coherently.

Since the decay of exciton population as well as exciton dephasing contributes to the homogeneous broadening [42], the derived decay time in our model may be directly translated into a homogeneous linewidth via a Fourier transform. A decay time of $\tau_c = 260$ fs corresponds to a homogeneous linewidth of 2.5 meV. However, the measured linewidth of the PL spectra [Fig. 1(b)] is 14 meV, because the excitonic resonances are inhomogeneously broadened [42]. Inhomogeneous line broadening in TMDCs may occur due to local potentials, which change the energy as well as the phase of the emitted light. These potentials are likely to arise from local charges in the environment, local strain, impurities, or vacancies. In addition, they may also undergo random temporal fluctuations on slower time scales in comparison to the femtosecond emission dynamics. These fluctuations cause a loss of coherence of the emitted light. However, the emission from both valleys originating from the same spatial position is affected in the same way by the inhomogeneities. In this way, the coherence of the emission from within one valley (intravalley coherence) is lost, while the intervalley coherence is still preserved. To model the inhomogeneous broadening in our calculation, we extend Eq. (1) with a superposition of an ensemble of damped harmonic oscillators with different energies $E_i = E_{K^\pm} + \Delta E_i$, whose amplitudes follow a Gaussian distribution with $\sigma = 14\ \mathrm{meV}/(2\sqrt{2\ln 2})$ centered at the exciton energies in Fig. 1(c) (see Supplemental Material for details [41]). Since the contributions of inhomogeneous broadening are of an incoherent nature, their inclusion in the model has no influence on the interpretation of the decay dynamics. Hence, the fitting parameters obtained before remain valid. Photoluminescence spectra are calculated by a fast Fourier transform of the electric field obtained from our extended model including broadening effects [Eqs. (S1)], projected onto the transmission axis of the analyzer. Figure 4 shows a comparison of the experimentally obtained photoluminescence spectra as a function of the analyzer angle for a magnetic field of 25 T with the corresponding spectra obtained from the model. The general spectral features as well as a shift of the first intensity maximum to 35° are well reproduced by our model. Interestingly, the center of the photoluminescence emission experiences a slightly stronger magnetic-field-induced rotation of emission polarization than the wings. This is because the corresponding left and right circularly polarized emission components from both valleys are different in intensity as one moves from the center towards the wings of the emission spectrum [see Fig. 1(a)].

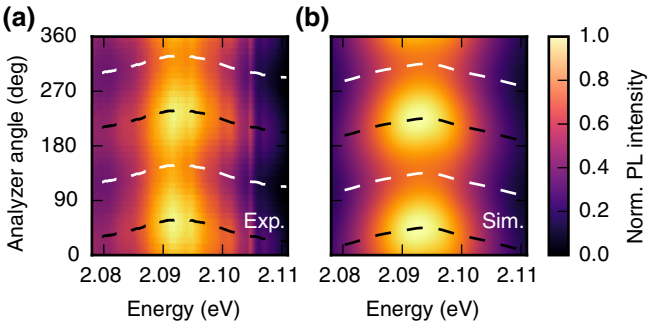

FIG. 4. (a) Measured and (b) calculated photoluminescence spectra of the neutral exciton of monolayer WS_2 at $B = 25$ T, as a function of the analyzer angle. The dashed white (black) lines indicate the analyzer angle for minimum (maximum) photoluminescence at each energy, showing a smaller rotation at the wings of the spectral line.

In conclusion, we have demonstrated how an out-of-plane magnetic field affects the coherent light emission from the valleys in a WS_2 monolayer. The linear polarization state of the emitted light rotates with respect to the excitation polarization, and the degree of polarization is

reduced with an increasing magnetic field. The observed phenomena arise due to the energy difference of the two emission components induced by the valley Zeeman splitting and depend on the decay time of the coherent emission. Therefore, an external magnetic field provides a way to manipulate the valley coherence via the valley Zeeman effect. However, the reported phenomena are of a general nature, because they are not limited to the material WS_2 and other mechanisms capable of lifting the valley degeneracy can be readily envisioned for controlling the valley coherence (e.g., the valley-selective optical Stark effect [46]), even on femtosecond time scales. In addition, our work paves the way towards the control and readout of the phase between valley excitons, which is important for the realization of valleytronic devices.

The authors gratefully acknowledge financial support by the A. v. Humboldt foundation, the DFG via GRK 1570, KO3612/1-1, and SFB689, and HFML-RU/FOM, a member of the European Magnetic Field Laboratory (EMFL).

R. S. and A. A. contributed equally to this work.

*Rudolf.Bratschitsch@uni-muenster.de

†Present address: Division of Physics and Applied Physics, School of Physical and Mathematical Sciences, Nanyang Technological University, Singapore 637371, Singapore.

[1] Q. H. Wang, K. Kalantar-Zadeh, A. Kis, J. N. Coleman, and M. S. Strano, Nat. Nanotechnol. **7**, 699 (2012).
[2] G. Eda and S. A. Maier, ACS Nano **7**, 5660 (2013).
[3] S. Z. Butler *et al.*, ACS Nano **7**, 2898 (2013).
[4] A. Splendiani, L. Sun, Y. Zhang, T. Li, J. Kim, C.-Y. Chim, G. Galli, and F. Wang, Nano Lett. **10**, 1271 (2010).
[5] K. F. Mak, C. Lee, J. Hone, J. Shan, and T. F. Heinz, Phys. Rev. Lett. **105**, 136805 (2010).
[6] W. Zhao, Z. Ghorannevis, L. Chu, M. Toh, C. Kloc, P.-H. Tan, and G. Eda, ACS Nano **7**, 791 (2013).
[7] P. Tonndorf, R. Schmidt, P. Böttger, X. Zhang, J. Börner, A. Liebig, M. Albrecht, C. Kloc, O. Gordan, D. R. T. Zahn, S. Michaelis de Vasconcellos, and R. Bratschitsch, Opt. Express **21**, 4908 (2013).
[8] I. G. Lezama, A. Arora, A. Ubaldini, C. Barreteau, E. Giannini, M. Potemski, and A. F. Morpurgo, Nano Lett. **15**, 2336 (2015).
[9] A. Arora, M. Koperski, K. Nogajewski, J. Marcus, C. Faugeras, and M. Potemski, Nanoscale **7**, 10421 (2015).
[10] A. Arora, K. Nogajewski, M. Molas, M. Koperski, and M. Potemski, Nanoscale **7**, 20769 (2015).
[11] K. F. Mak, K. He, J. Shan, and T. F. Heinz, Nat. Nanotechnol. **7**, 494 (2012).
[12] G. Sallen, L. Bouet, X. Marie, G. Wang, C. R. Zhu, W. P. Han, Y. Lu, P. H. Tan, T. Amand, B. L. Liu, and B. Urbaszek, Phys. Rev. B **86**, 081301 (2012).
[13] T. Cao, G. Wang, W. Han, H. Ye, C. Zhu, J. Shi, Q. Niu, P. Tan, E. Wang, B. Liu, and J. Feng, Nat. Commun. **3**, 887 (2012).
[14] H. Zeng, J. Dai, W. Yao, D. Xiao, and X. Cui, Nat. Nanotechnol. **7**, 490 (2012).
[15] G. Kioseoglou, A. T. Hanbicki, M. Currie, A. L. Friedman, D. Gunlycke, and B. T. Jonker, Appl. Phys. Lett. **101**, 221907 (2012).
[16] A. M. Jones, H. Yu, N. J. Ghimire, S. Wu, G. Aivazian, J. S. Ross, B. Zhao, J. Yan, D. G. Mandrus, D. Xiao, W. Yao, and X. Xu, Nat. Nanotechnol. **8**, 634 (2013).
[17] C. R. Zhu, K. Zhang, M. Glazov, B. Urbaszek, T. Amand, Z. W. Ji, B. L. Liu, and X. Marie, Phys. Rev. B **90**, 161302 (2014).
[18] G. Wang, X. Marie, I. Gerber, T. Amand, D. Lagarde, L. Bouet, M. Vidal, A. Balocchi, and B. Urbaszek, Phys. Rev. Lett. **114**, 097403 (2015).
[19] A. Pospischil, M. M. Furchi, and T. Mueller, Nat. Nanotechnol. **9**, 257 (2014).
[20] B. W. H. Baugher, H. O. H. Churchill, Y. Yang, and P. Jarillo-Herrero, Nat. Nanotechnol. **9**, 262 (2014).
[21] J. S. Ross, P. Klement, A. M. Jones, N. J. Ghimire, J. Yan, D. G. Mandrus, T. Taniguchi, K. Watanabe, K. Kitamura, W. Yao, D. H. Cobden, and X. Xu, Nat. Nanotechnol. **9**, 268 (2014).
[22] P. Tonndorf, R. Schmidt, R. Schneider, J. Kern, M. Buscema, G. A. Steele, A. Castellanos-Gomez, H. S. J. van der Zant, S. Michaelis de Vasconcellos, and R. Bratschitsch, Optica **2**, 347 (2015).
[23] M. Koperski, K. Nogajewski, A. Arora, V. Cherkez, P. Mallet, J.-Y. Veuillen, J. Marcus, P. Kossacki, and M. Potemski, Nat. Nanotechnol. **10**, 503 (2015).
[24] A. Srivastava, M. Sidler, A. V. Allain, D. S. Lembke, A. Kis, and A. Imamoğlu, Nat. Nanotechnol. **10**, 491 (2015).
[25] Y.-M. He, G. Clark, J. R. Schaibley, Y. He, M.-C. Chen, Y.-J. Wei, X. Ding, Q. Zhang, W. Yao, X. Xu, C.-Y. Lu, and J.-W. Pan, Nat. Nanotechnol. **10**, 497 (2015).
[26] C. Chakraborty, L. Kinnischtzke, K. M. Goodfellow, R. Beams, and A. N. Vamivakas, Nat. Nanotechnol. **10**, 507 (2015).
[27] K. Behnia, Nat. Nanotechnol. **7**, 488 (2012).
[28] S. L. Adler, Ann. Phys. (N.Y.) **67**, 599 (1971).
[29] G. Busch, Physica (Amsterdam) **89B+C**, 1 (1977).
[30] R. Macêdo, R. L. Stamps, and T. Dumelow, Opt. Express **22**, 28467 (2014).
[31] R. Macêdo and T. Dumelow, Phys. Rev. B **89**, 035135 (2014).
[32] *High Magnetic Fields in Semiconductor Physics II*, edited by G. Landwehr, Springer Series in Solid-State Sciences Vol. 87 (Springer, Berlin, 1989).
[33] Y. Li, J. Ludwig, T. Low, A. Chernikov, X. Cui, G. Arefe, Y. D. Kim, A. M. van der Zande, A. Rigosi, H. M. Hill, S. H. Kim, J. Hone, Z. Li, D. Smirnov, and T. F. Heinz, Phys. Rev. Lett. **113**, 266804 (2014).
[34] G. Aivazian, Z. Gong, A. M. Jones, R.-L. Chu, J. Yan, D. G. Mandrus, C. Zhang, D. Cobden, W. Yao, and X. Xu, Nat. Phys. **11**, 148 (2015).
[35] A. Srivastava, M. Sidler, A. V. Allain, D. S. Lembke, A. Kis, and A. Imamoğlu, Nat. Phys. **11**, 141 (2015).
[36] D. MacNeill, C. Heikes, K. F. Mak, Z. Anderson, A. Kormányos, V. Zólyomi, J. Park, and D. C. Ralph, Phys. Rev. Lett. **114**, 037401 (2015).
[37] G. Wang, L. Bouet, M. M. Glazov, T. Amand, E. L. Ivchenko, E. Palleau, X. Marie, and B. Urbaszek, 2D Mater. **2**, 034002 (2015).

[38] A. A. Mitioglu, P. Plochocka, Á. Granados del Aguila, P. C. M. Christianen, G. Deligeorgis, S. Anghel, L. Kulyuk, and D. K. Maude, Nano Lett. **15**, 4387 (2015).

[39] A. V. Stier, K. M. McCreary, B. T. Jonker, J. Kono, and S. A. Crooker, Nat. Commun. **7**, 10643 (2016).

[40] G. Plechinger, P. Nagler, J. Kraus, N. Paradiso, C. Strunk, C. Schüller, and T. Korn, Phys. Status Solidi RRL **9**, 457 (2015).

[41] See Supplemental Material at http://link.aps.org/supplemental/10.1103/PhysRevLett.117.077402 for the polarization patterns for all measured magnetic fields, a method to correct Faraday rotation, and technical details about the theoretical modeling.

[42] G. Moody, C. K. Dass, K. Hao, C.-H. Chen, L.-J. Li, A. Singh, K. Tran, G. Clark, X. Xu, G. Berghäuser, E. Malic, A. Knorr, and X. Li, Nat. Commun. **6**, 8315 (2015).

[43] C. Poellmann, P. Steinleitner, U. Leierseder, P. Nagler, G. Plechinger, M. Porer, R. Bratschitsch, C. Schüller, T. Korn, and R. Huber, Nat. Mater. **14**, 889 (2015).

[44] K. Hao, G. Moody, F. Wu, C. K. Dass, L. Xu, C.-H. Chen, L. Sun, M.-Y. Li, L.-J. Li, A. H. MacDonald, and X. Li, Nat. Phys. **12**, 677 (2016).

[45] M. Palummo, M. Bernardi, and J. C. Grossman, Nano Lett. **15**, 2794 (2015).

[46] E. J. Sie, J. W. McIver, Y.-H. Lee, L. Fu, J. Kong, and N. Gedik, Nat. Mater. **14**, 290 (2014).